Thermal Analysis of Potted Litz Wire for High-Power-Density Aerospace Electric Machines

Andrew A. Woodworth,[1] Andrew Smith,[2] William Sixel,[3] Ryan Edwards,[4] and Ralph Jansen[5]
NASA Glenn Research Center, Cleveland, Ohio 44135 USA

Sean McCormick[6]
NASA Langley Research Center, Hampton Virginia 23666 USA

Malcolm Robbie[7] and Gerald Szpak[8]
V*antage Partner LLC Brook Park Ohio 44142 USA*

Paria Naghipour[9] and Euy-Sik Shin[10]
Ohio Aerospace Institute, Cleveland, Ohio 44142 USA

Abstract: Increasing the power density and efficiency of electric machines (motors and generators) is integral to bringing electrified aircraft (EA) to commercial realization. To accomplish that, an effort to create a high-efficiency megawatt motor (HEMM) with a goal of exceeding 98% efficiency and 1.46 MW of power has been undertaken at the NASA Glenn Research Center. Of the motor components, the resistive losses in the stator windings are by far the largest contributor (34%) to total loss in the motor. The challenge is the linear relationship between resistivity and temperature, making machine operation sensitive to temperature increases. In order to accurately predict the thermal behavior of the stator, the thermal conductivity of the Litz wire-potting-electrical insulation system must be known. Unfortunately, this multimaterial system has a wide range of thermal conductivities (0.1 – 400 W/m·K) and a high anisotropy (axial vs. transverse), making the prediction of the transverse thermal conductivity, and thus the hot-spot temperatures in the windings, difficult. To do this, a device that simulates the thermal environment found in the HEMM stator was designed. This paper discusses the design, thermal heat conjugate analysis (thermal model), manufacturing, and testing of HEMM's statorette. Results are analyzed by thermal resistance network modeling and microthermal modeling and are compared to analytical predictions of thermal conductivity of the insulated and potted Litz wire system.

I. Nomenclature

K	=	thermal conductivity
$K11$	=	longitudinal thermal conductivity parallel to the conductor
$K22$	=	transverse thermal conductivity
$K33$	=	through-thickness thermal conductivity
I	=	electrical current

[1] Research Physicist, Materials Chemistry and Physics Branch/ Materials and Structures Division, AIAA Member
[2] Mechanical Engineer, AIAA Member
[3] Pathways Intern, Thermal Systems and Transport Processes Branch/ Propulsion Division, AIAA Member
[4] Thermal Engineer, Thermal Systems and Transport Processes Branch/ Propulsion Division, non-member
[5] Technical Management, Aeronautics Mission Office, AIAA Member
[6] Mechanical Engineer, Aeronautics Systems Engineering Branch, non-member
[7] Lead Engineer, non-member
[8] Mechanical Engineer IV, non-member
[9] Research Associate, Multiphysics and Multi Scale Modeling Branch, AIAA Member
[10] Principal Scientist, Research Team Manager-Materials, AIAA Member

R = electrical resistance
x_2, x_3 = transverse directions, perpendicular to the longitudinal fiber (conductor)

II. Introduction

Increasing the power density and efficiency of electric machines (motors and generators) is integral to bringing Electrified Aircraft (EA) to commercial realization [1]. To accomplish that, an effort to create a High Efficiency Megawatt Motor (HEMM) with a goal of exceeding 98% efficiency and 1.46 MW of power has been undertaken by Jansen et. al. [2] at the NASA Glenn Research Center. Of the components, resistive (I^2R) losses in the stator windings are by far the largest (34%) contributor to this design's total energy losses. As discussed in a previous paper [3], the challenge is the linear relationship between resistivity and temperature that makes machine operation sensitive to temperature increases. This is demonstrated by a simple calculation that reveals a 1 °C increase in temperature results in a 0.39% decrease in efficiency. In order to accurately predict the thermal behavior of the stator, the thermal conductivity of the Litz wire-potting-electrical insulation systems must be known. In the HEMM design (internal rotor) the stator comprises a soft magnetic material and very narrow teeth designed primarily for heat removal from the windings. The soft magnetic material, also referred to as the back-iron, has cooling channels build into the material towards the outside diameter of the structure. The windings consist of type 8 Litz wire (American Wire Gauge (AWG) 3 equivalent). Each slot holds two windings each in a double wrap of high voltage insulating material. The Litz wire consist of 6000 AWG 40 (~80-μm-diameter) copper strands, each insulated with a single build coating of MW 16-C polyimide insulation. The entire winding stator package is potted using epoxy. The system has a top operation temperature of 220 °C because of the temperature limits of the insulation packages. The windings fill up most of the slot, but leave a little room at the top which forms cannels for direct liquid cooling. The rotor consist of superconducting field windings that are cooled by a rotating cryocooler. Unfortunately, this is a multimaterial system with a wide range of thermal conductivities (0.1 – 400 W/m·K) and a high anisotropy (axial vs. transverse) [3, 4]. Therefore, predicting the transverse thermal conductivity that, in turn, determines the hot-spot temperatures in the windings is difficult.

In order to accurately measure the thermal conductivities of the system, a device that simulates the thermal environment found in the HEMM stator was designed. This device is like motorettes (little motors) that are described in IEEE standards for testing electrical insulation lifetimes and are found in other electric motor testing. However, because the HEMM motor design also includes significant rotor electrical and thermal considerations, the term "motorette" was not deemed appropriate. Instead, "statorette" (or little stator) was adopted as the term for this test device. This paper discusses the design, thermal heat conjugate analysis (thermal model), manufacturing, and testing of HEMM's statorette. The results are compared to the predictions of the thermal model, and a microthermal model is developed to further understand the transverse heat flow through the potted Litz wire.

III. Experimental Design and Build

A. Design

The statorette (Fig. 1) was designed to mimic the thermal environment of the stator as closely as possible. The HEMM stator is a semi-slot-less design [5] that consists of a type 8 Litz wire wound through laminated soft magnetic slots with thin teeth. The teeth provide both mechanical stability of the system and a thermal pathway. Each slot contains two Litz wire windings. Cooling of the stator is achieved by passing a liquid over the windings and through the soft magnetic material. To replicate this environment a race track configuration (Fig. 1(a)) was chosen. The design contains three individual tracks each with two wires in each slot. The three-track design was chosen so that the middle track would look as thermally close to the real stator as possible. Specifically, joule heating will occur in both of the wires in the center slot, and heat will also be generated in both of the adjoining slots. Therefore, the heating in the middle slot and end winding should be accurate to at least the first order. The statorette was also designed to accommodate the fluid flow. The stator is designed with fluid channels over exposed wires in slots and a return path through the soft magnetic material. The fluid (Fig. 1(c)) comes in over the top of the end turns and flows through Litz wire channels around the opposite end turns, through the cooling/flow holes in the laminated soft magnetic material, and finally past the bottom side of the end turns before exiting the stator. This same configuration is replicated in the statorette.

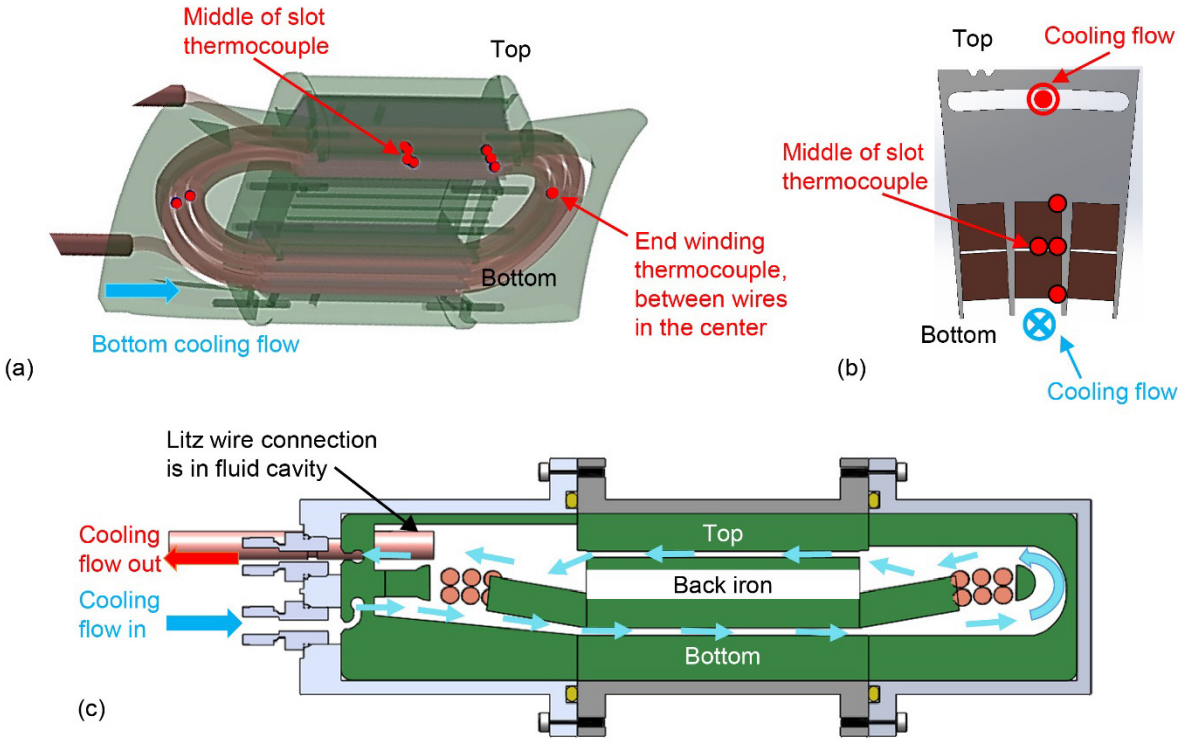

Fig. 1 Statorette design. Bottom refers to where the air gap/rotor would be placed and top is representative of the outside of the stator. Thermocouple locations are marked in red. Data from the marked slot and end winding thermal couples are used in the discussion section. (a) Overall design of statorette with Litz wire windings. (b) Axial cross section of a set of three slots with two Litz wire bundles in each slot. (c) Cooling flow path.

The slots are made out of a laminated steel alloy that closely mimics the thermal characteristics of the cobalt-iron chosen for the stator (transvers thermal conductivity ~27 W/m·k). The rest of the housing is made from three-dimensional (3-D) printed plastic. The 3-D printed parts allow for fast prototyping and also are also of low thermal conductivity (~0.1 W/m·K) so that only the metal slot portions contribute to thermal conduction. Because this is only a small portion of the stator, U-shaped plastic pieces were inserted to represent missing windings that contribute to forming the flow path. The Litz wire consists of a base AWG 40 (79.9-μm-diameter) wire with a heavy built MW-16 polyimide (240 °C rating) build. 1500 individual wires were twisted into bundles, and then a structural nylon serve was put around the bundle. Four of these of these bundles (6000 total individual wires) were twisted together and then put through an 8-mm × 8-mm die. The resulting square wire was then double wrapped in a synthetic aromatic polyamide polymer fiber serve that is the basis of the high-voltage insulation (turn-to-turn and turn-to-ground). Type K thermocouples are placed in the middle slot as shown in Figs. 1(a) and (b). Thermocouple locations were based on thermal modeling as discussed in Section III, Results and Discussion.

B. Build

The laminated metal slots were impregnated with a high-temperature (260 °C) two-part epoxy with no fillers and a thermal conductivity of 1.3 W/m·K using vacuum pressure impregnation (VPI). After epoxy impregnation, the laminated metal slots were fixed into the plastic housing using room-temperature-vulcanizing (RTV) silicone. RTV silicone was chosen to help alleviate stress caused by thermal coefficient of expansion mismatch between the metal laminates and plastic parts. Winding was accomplished using a single piece of Litz wire that was wrapped six times around the statorette, filling the bottoms of the slots and then the top. The wires were set into the slots using a hammer and block in order to maximize their packing density. The ends of the Litz wire were stripped using a buffered molten sodium hydroxide solution followed by a citric acid sonic bath cleaning. Further removal of residual organic material was done by sonicating the stripped Litz wire ends using methyl ethyl ketone, acetone, and propanol (in that order). Connecting lugs were crimped and then soldered onto the ends of the wires using a resistive soldering and a eutectic Sn-Pb solder paste with added flux. An additional fixture was added to aid in locating the connecting lugs during the potting process.

The entire assembly was potted using the same two-part epoxy used to impregnate the metal laminations. However, the VPI process was heavily modified in order to fully infiltrate the Litz wire bundles (micrometer-sized area) and also fill large voids (millimeter-sized) around the bundles without the epoxy draining out during the curing process. This was accomplished by determining the viscosity-temperature-time relationship using both spindle and parallel plate rheology measurement techniques. The entire unit was preheated to 60 °C to drive off excess moisture and then suspended in the VPI chamber above the epoxy bath. The chamber was closed and evacuated to ~1 Torr, and the epoxy temperature was raised to 50 °C. Raising the epoxy temperature reduces the viscosity and aids in outgassing of volatiles that cause voids in the final product. Once outgassing the epoxy is complete (no or insignificant amount of bubbling of the epoxy visible), the part is immersed in the epoxy bath. A period of time is provided for additional outgassing resulting from the immersion of the part to occur. After fully outgassing, pressure is applied (~85 psi), and the temperature of the epoxy and part are raised again. Raising the temperature again lowers the viscosity (enhances infiltration), but also shortens the working time of the epoxy. As the epoxy reaches the end of the working time its viscosity increases, which keeps it from flowing out of the larger (millimeter-sized) voids during the curing process. Once the desired epoxy viscosity has been reached, the part is removed from the VPI chamber and put through the epoxy manufacturer's recommended cure cycle in a forced convection oven.

After the potting process is completed the locating fixture and excess epoxy are removed. Gaps between the end windings and plastic flow pieces were filled with RTV to ensure the cooling fluid follows the proper and then statorette is fit into the fluids housing. Compression style fittings were used to create fluid tight feedthroughs for both the connecting lugs and thermocouple wires. Additional thermal couples were placed in the connecting lugs, inlet and outlet fluid flows (directly out dis of the fluid cavity) to properly capture data necessary to do a proper energy balance of the test. Jensen et al. [2] identified a 60 °C cooling loop as the most likely cooling source for the motor on an aircraft, and therefore 60 °C was adopted as the baseline coolant temperature for the motor. A silicone oil rated for use in transformers was chosen as the coolant with a viscosity of 25–35 cSt at operational temperature and a published room-temperature thermal conductivity of 0.151 W/m·K. Initial computational fluid dynamics (CFD) flow models predicted a laminar flow and that a point of diminishing returns is reached when flows exceeded ~8 liter/min. To test this hypothesis three flows were chosen: 4.36, 8.2, and 11.8 liter/min. The oil is delivered to the test section by a custom build supply that regulates the temperature of the input fluid while supplying a constant pressure and flow rate. A direct current was supplied to the statorette from 0–500 A. The HEMM motor is designed to run with 400 A, but the test ran up to 500 A in order to account for inductive heating of the soft magnetic material and possible motor transients that will cause additional heating.

IV. Conjugate Heat Transfer Analysis

A thermal model of the statorette was assembled in CFD software [6]. The model consisted of two multiphysics modules: A conjugate CFD heat transfer study accepted flow and assembly heat flux parameters, producing a steady-state flow field and surface heat transfer characteristics (local heat transfer coefficients, and near-wall temperatures). Data from the CFD heat transfer study was then used to populate a solids-only assembly in finite element analysis (FEA) software [7], where the non-isotropic heat transport properties of the participating bodies could be represented in high fidelity.

A simplified flow geometry was used to represent the critical heat transfer interfaces, flow restrictions, turns, and boundary conditions. Only thermally participating solid bodies were modeled—including the encapsulated Litz wire turns and laminated steel slots. The 3-D printed plastic bodies that define the statorette flow cavity were omitted from the analysis, as they were not in the heat conduction path between the wire bundles and circulating fluid.

The fluid domain material properties (Table 1) were transcribed directly from the silicon oil manufacturer's specification sheet [8], including temperature-dependent viscosity, isothermal specific heat, density, and linear thermal expansion coefficient. The CFD 2 (Fig. 2) model yielded steady-state non-isothermal flow solutions for each prescribed coil heat flux (W), and silicone oil flow rate (liters/min).

Using the temperature difference between two thermal couples embedded in the slot section, the transverse thermal conductivity of the potted Litz wire was determined to be 3.4 W/m·K. Using a model from Simpson et al. [9] for impregnated wire and the vendor-provided packing factor of the copper filaments in the Litz wire of 0.54 resulted in the thermal conductivity of 2.75 W/m·K. However, cross-sectional analysis of the wire (Table 2, Litz2 [10]) revealed that the packing fraction averaged from 0.55–0.78 with an average packing density of 0.68. Using the observed average packing density of 0.68 results in a thermal conductivity of 3.6 W/m·K. Using the two calculated values as bounding cases yielded positive correlation between the calculated and observed values. The extracted surface heat transfer characteristics were applied to the solids-only thermal model, with a typical Litz bundle transverse conductivity of

3.4 W/m·°C. A thermal solution was produced for a sweep of oil flow rate (4.36, 8.2, and 11.8 liter/min) and coil heat dissipation (126–1048 W, corresponding to 100–500 A). Peak wire temperatures were reported as a function of flow rate and current for the laminated slots (Fig. 3 (b)) and end-turns (Fig. 3(a)).

Table 1: Silicon Oil Properties [8]

Specific gravity	0.985	Refractive index	1.425
Pour point, °C	–57	Surface tension	25
Flash point, °C	275	Auto-ignition temperature, °C	482
Specific heat at 100 °C	0.405		
Thermal conductivity at 25 °C, W/m·k	0.15	Coefficient of thermal expansion from 1 to 100 °C, 1/K	0.00096

Viscosity, cSt	Temperature, °C
50	25
38	38
14	99

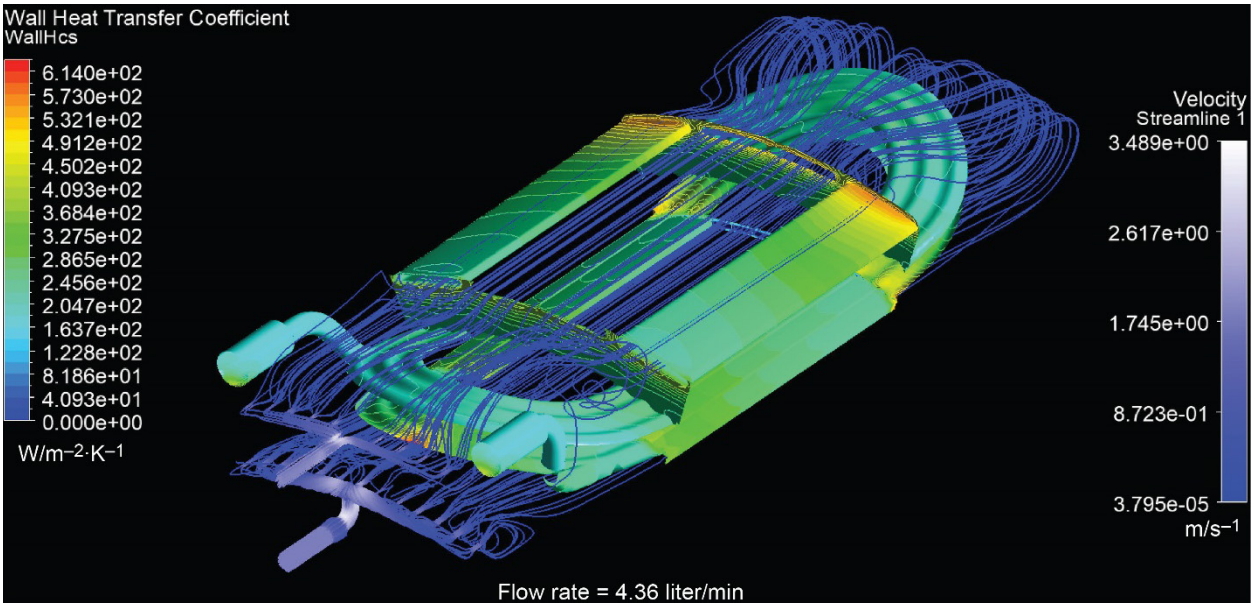

Fig. 2 Statorette flow solution and heat transfer characterization for 4.36 liter/min.

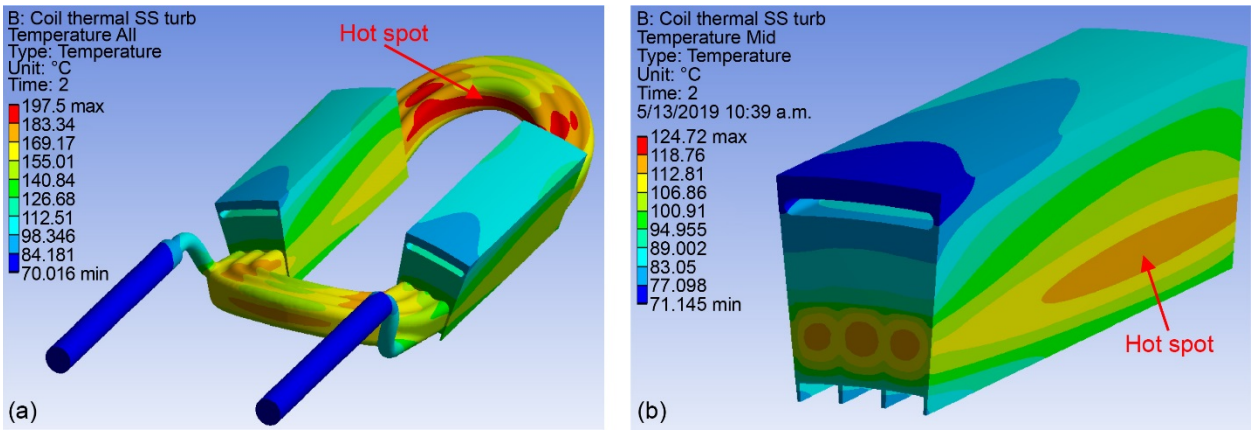

Fig. 3 Statorette thermal solution for 4.36 liter/min, 500 A (1048 W) (a) Full winding and (b) detail of laminated slot with Litz wire.

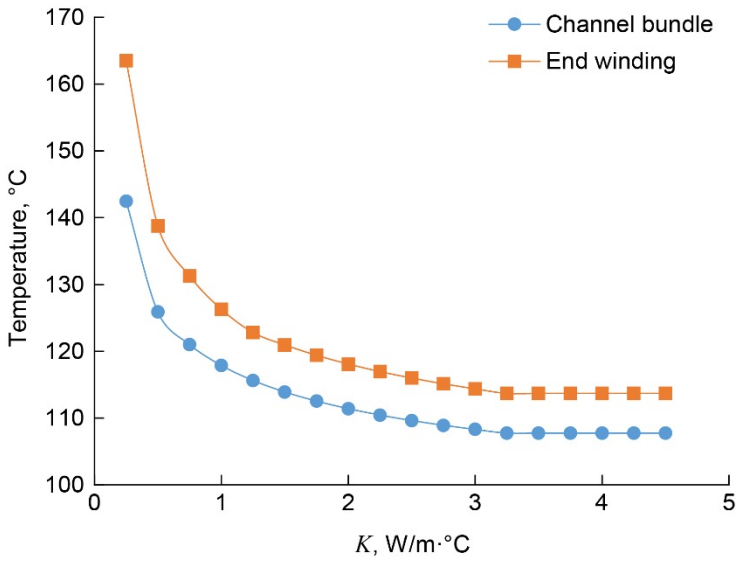

Fig. 4 Finite-element-modeled Litz bundle temperature sensitivity to thermal conductivity at 400 A (600 W) and 8.2 liters/min.

Wire temperatures were predicted to fall below the 200 °C limit for all combinations of oil flow rate and assembly heat fluxes. A follow up study (Fig. 4) was conducted with the experimentally-validated heat transfer model, to assess model sensitivity to Litz bundle thermal conductivity. A sweep of the transverse component of the encapsulated bundle conductivity was performed across a relatively wide range of 0.0.5–4.75 W/m·°C. Diminishing returns in Litz wire cooling (Fig. 4) are observed for transverse conductivities above ~3.5 W/m·°C, indicating that statorette cooling performance is limited by the convection heat transfer interface, rather than conduction through the solid members of the assembly.

V. Results and Discussions

The data from the test is shown in Fig. 4. In the statorette slot regions the hottest observed temperatures corresponded to the locations predicted by the thermal models. The hottest temperature observed in the slots was 186 °C (4.36 liter/min, 500 A), and the hottest observed end windings was 193 °C (4.36 liter/min, 500 A). This is well below the 220 °C limit of the insulation system. Data for all of thermocouples consistently shows a larger reduction in temperature between 4.36- and 8.2-liters/min flows than between 8.2- and 11.8-liters/min flows under 450 A (802 W), which is constant with the flow-cooling predictions. Although at 500 A (1048 W) this trend reverses and higher flow rates would need to be considered if the operation of the electric machine were to require those sort of currents and power. However, the HEMM machine is being designed for 400-A operation, and testing to 500 A demonstrates a design margin to account for possible transient currents and inductive heating from AC loss in the soft magnetic material of the stator slots (sometimes referred to as the “back iron”). Figs. 5(c) and (d) show a comparison of the of the thermal model predictions and test data for the 4.36-liter/min test case and show that both the slot and end turn measurements were in reasonable agreement with the model. The model underpredicted the slot temperature by 10.4 °C (5.6%) at 500 A, but only 5.3 °C (3.8%) at 400 A. The end turns hot spots were over predicted by 4.5 °C at (2.3%) and 3.7 °C (2.5%) at 400 A. One factor that was not properly accounted for in this model is the change in thermal conductivity of the cooling fluid with temperature. In-house analysis of the cooling oil measurements indicate that there is a 6.6% decrease in the thermal conductivity of the silicon oil at 60 °C; therefore, a thermal conductivity of 0.141 W/m·K will be used for future analysis. Also the difference in fluid flow in the different regions (slots vs. end windings) may also contribute to the differences in prediction.

The results suggest that the calculated transverse thermal conductivity of 3.4 W/m·k and analytically calculated value of 3.6 W/m·K reasonably represent the transvers thermal conductivity and that the values for the observed wire packing fraction (Table 2) are accurate for this application. Also, the results indicate that the cooling scheme for HEMM is sufficient and the material selection for potting provides adequate transvers thermal conductivity.

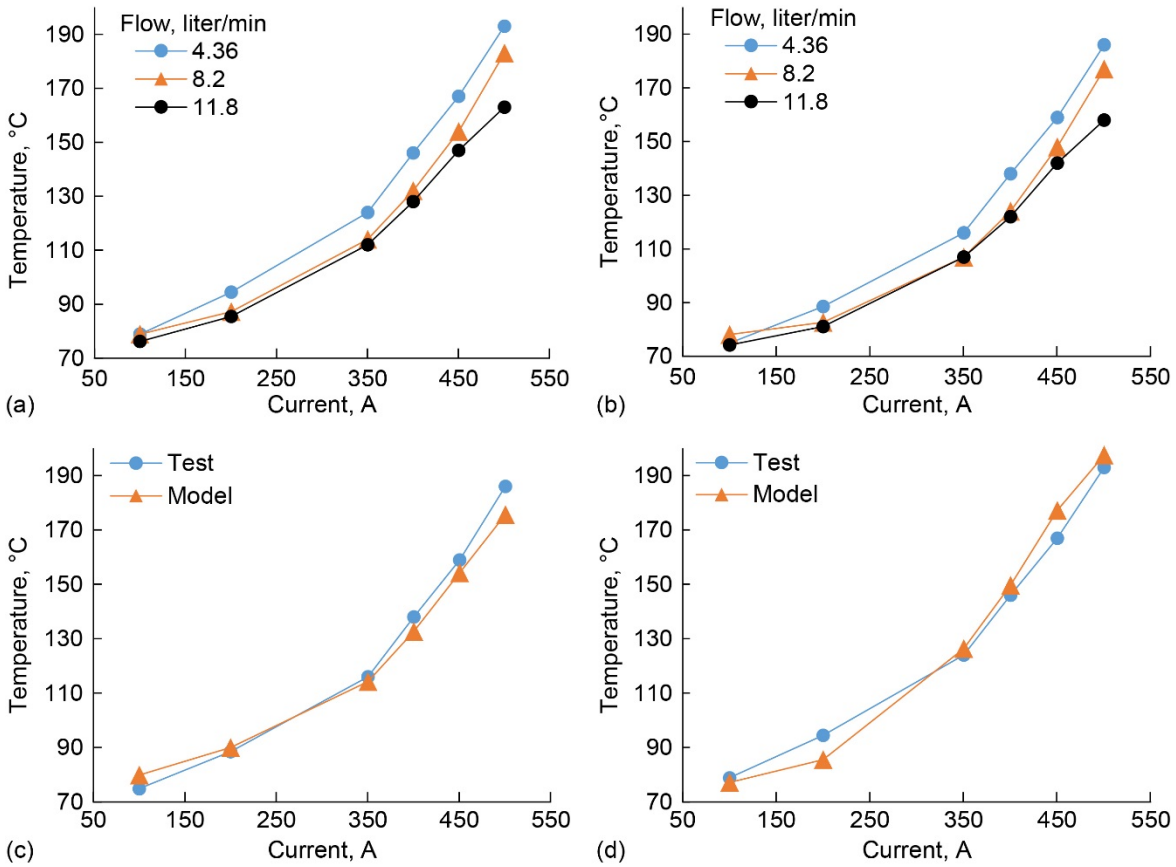

Fig. 5 Measured temperatures at expected hot spots the slots (a) and end windings (b). Comparison of thermal-model-predicted and measured hot spot temperatures for the 4.36-liter/min test case for the slots (c) and end windings (d).

Specifically, the transverse thermal conductivity is high enough that it is not limiting factor in thermal management of the stator as designed (thermal management scheme). Furthermore, if a standard epoxy (~0.1 W/m·K) had been used to impregnate (pot) the Litz wire the predicted transvers thermal conductivity, using the same analytical model as referenced earlier [9], would be 0.3 W/m·K, and would result in an increase of 50 °C in the end winding and 35 °C in the slots over the current temperatures. This would result in the end windings being greater than 180 °C at 400 A at a flow rate of 8.2 liter/min and most likely exceeding 200 °C at a flow rate of 4.36 liter/min. Therefore increasing the thermal conductivity of the impregnation/potting material up to/or above 1.3 W/m·K and packing the individual strands of the Litz wire a densely as possible is necessary for this design to meet its power density and efficiency targets.

Postanalysis (Fig. 6) of the potted Litz wire revealed that the slots and Litz wire were more than 90% (estimate) impregnated. However, the analysis did reveal millimeter-sized voids (Fig. 6(a)), which did travel the length slots and seem to be confined bubbles. Higher resolution optical micrographs (Fig. 6(c)) show that the wires are completely encapsulated and show good infiltration of the wires and interbundle spaces. The major exception was in the center of the bundle where in 95% of the examined cross sections examined a void was found (Fig. 6(b)). It was also common to find voids between the high-voltage wrap and the bundles where two bundles come together, as seen in Fig. 6(b). Finally, cross-sectional analysis of the end windings shown in Fig. 6(d) revealed large voids between the wires where either stagnant cooling fluid would sit or in some cases air gaps may possibly exist. Because the HEMM design requires large end windings, this finding is particularly troubling, however it did not prevent statorette from operating at 500 A with maximum recorded temperatures below 200 °C, but it does bring into question if the thermal couple was indeed reading the sign of the maximum temperature. Many of the millimeter-sized gaps may be solved by cycling pressure and vacuum while waiting for the epoxy to raise in viscosity. As for the large voids in the end windings, either the viscosity needs to be greater before removal from the epoxy bath or another round of epoxy needs to be applied in a separate process.

Table 2: Quantitative image analysis results of microstructures of potted Litz wires from Fig. 8 [10]

Litz wire type		Areal fraction			Coating thickness, μm
		Cu filament	Coating	Open space	
Litz1	**All bundles**	75.9±1.2%		24.2±1.2%	
Litz2	**B1-1**	67.8%	14.2%	18.0%	4.13±1.3
	B2-1	60.0%	14.6%	25.3%	4.37±1.8
	B3-1	62.0%	15.1%	22.9%	4.23±1.0
	B4-1	55.2%	13.8%	31.0%	4.26±1.3
	Avg.	61.3±5.2%	14.4±0.6%	24.3±5.4%	4.26±0.1
	B1-2	73.2%	16.4%	10.4%	3.77±1.0
	B2-2	74.3%	14.9%	10.8%	3.46±0.7
	B3-2	75.0%	16.7%	8.3%	3.73±0.7
	B4-2	76.1%	16.6%	7.3%	3.66±0.8
	Avg.	74.7±1.2%	16.2±0.8%	9.2±1.7%	3.65±0.1
	Total avg.	68.0±8.0%	15.3±1.1%	17.0±8.9%	3.98±0.34

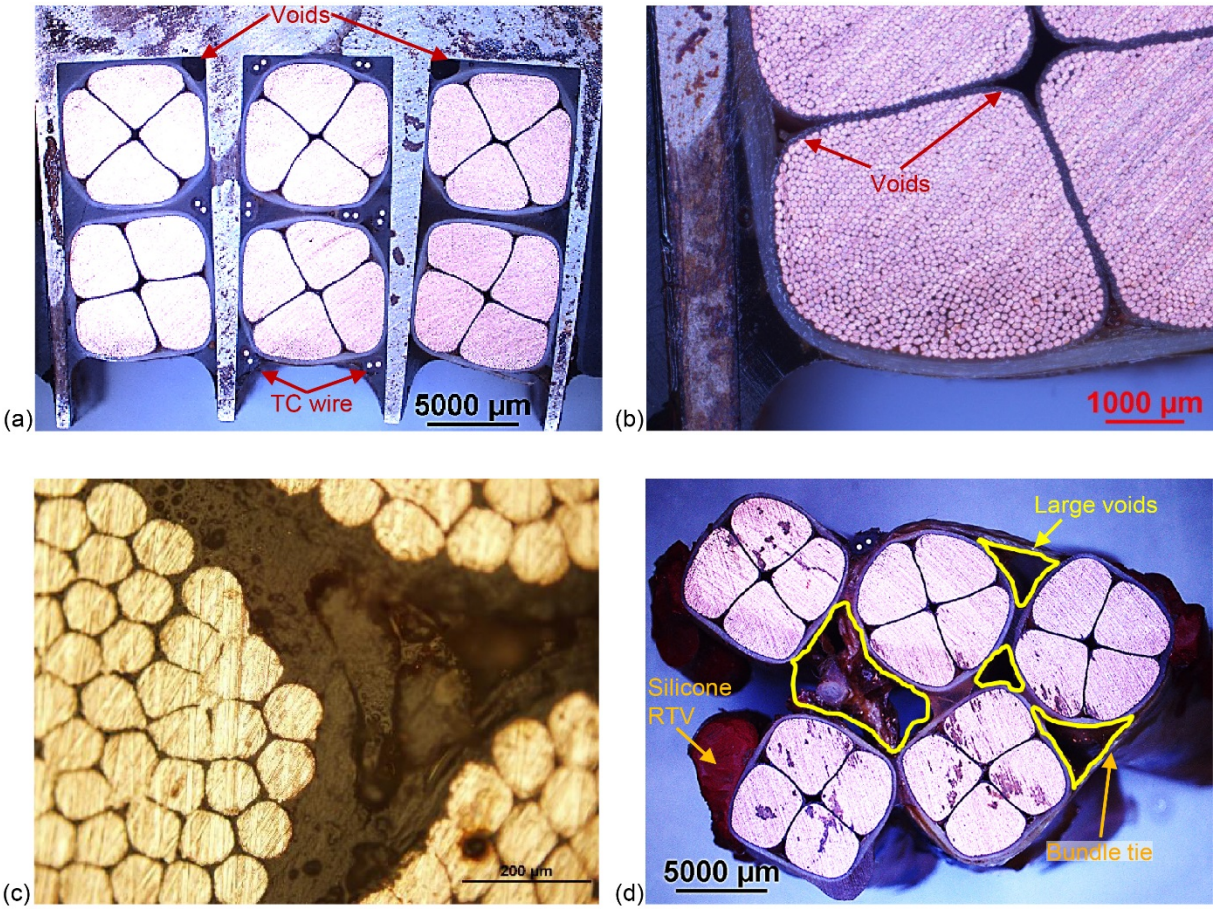

Fig. 6 Cross-sectional analysis of a potted statorette. (a) Full cross section of a laminated slot; TC is thermocouple. (b) Closeup of a single Litz wire in a slot. (c) High-magnification image of the center of a Litz wire in slot. (d) Cross section of an end winding.

VI. Microthermal Analysis

In order to better understand the how heat flows through the volume of the Litz wire a microthermal model is currently under development [3]. The main advantage of a microthermal model is that it incorporates the structural details of the Litz wire such as the packing of the individual wires, volume fractions of individual wire constituents, (conductor, potting material, and insulator), and constituent size. The influence of the above-mentioned structural details on thermal conductivity and heat flux distribution can be easily investigated through this ultra-efficient microthermal model. The details of a microthermal model incorporating the structural details of the Litz wire such as the packing of the individual wires, volume fractions of individual wire constituents, (conductor, potting material, and insulator), and constituent size is presented in this section. High fidelity generalized method of cells (HFGMC), utilized for the microthermal model here, is a higher order refined micromechanical theory extended by vector constitutive laws and is capable of predicting effective properties (thermal conductivities) and local field distributions (heat flux) in a multiphase system [11]. Unlike general classical numerical methods such as FEA, the HFGMC is tailored towards periodic multiphase media. Periodicity is imposed through continuity of displacements and tractions in an average sense at the surface of the RUC. This micromechanics microthermal tool aims to strike a balance between simplicity, accuracy, and efficiency without the need for excessive computational power.

Fig. 7 shows a realistic representative unit cell (RUC) of the three-phase media in a Litz wire (left) regenerated numerically through a MATLAB routine (right) [12]. The output of this MATLAB routine produces micromechanical inputs for the HFGMC micromechanics code. The produced input file comprises the numbers 1, 2, and 3 that represent the filament, insulator coating, and potting material, respectively. It only needs some manual modification by the user to fit the HFGMC template for producing results. Once the input file is constructed correctly, conductivity and heat flux can be calculated in the code utilizing this input and extended vector constitutive laws. Although the wire arrangements might not be a perfect representation of the conductor filaments in a Litz wire bundle, they provide a chance to take a deeper look into the influence of geometrical arrangements on overall system performance. For a given conductor diameter/volume ratio, the microstructural arrangement (packing) can be varied (see upcoming example pictures) to assess the influence on thermal conductivity and heat flux.

The Litz2 wire was examined [10] for its packing density after being potted with a 2-part epoxy (Fig. 8 and Table 2). The Litz2 wire was selected for use in HEMM and used in the statorette test previously described. Comparison of the builds and intrabundle differences give detailed information on what might be expected from different Litz wires. Figs. 9 and10 show the preliminary thermal conductivity and heat flux results obtained through the microthermal

(a) 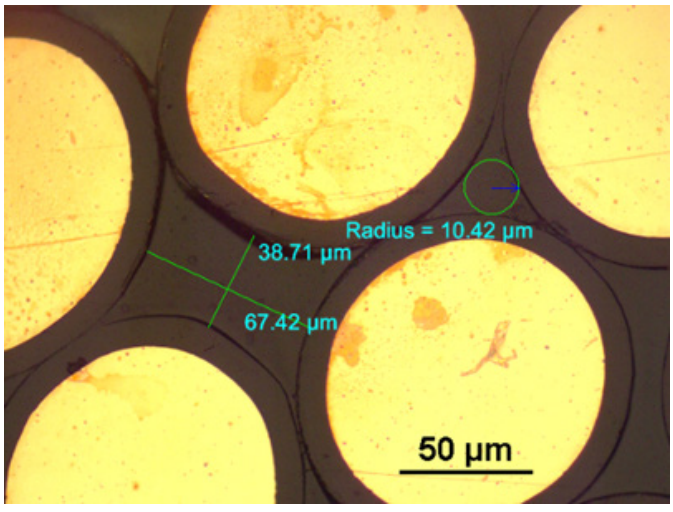

(b) 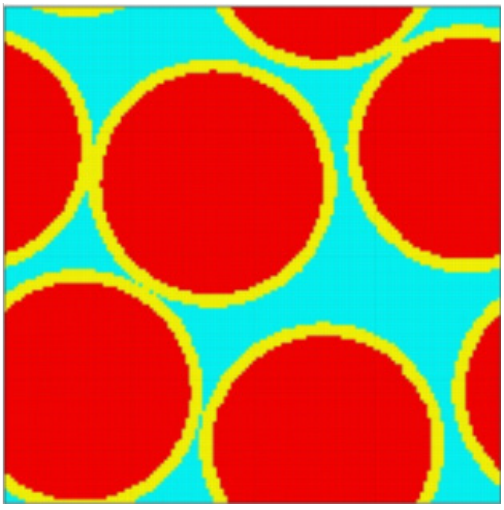

Fig. 7 Representative unit cell (RUC) of the three-phase media in a Litz wire (a) regenerated numerically through a MATLAB routine (b).

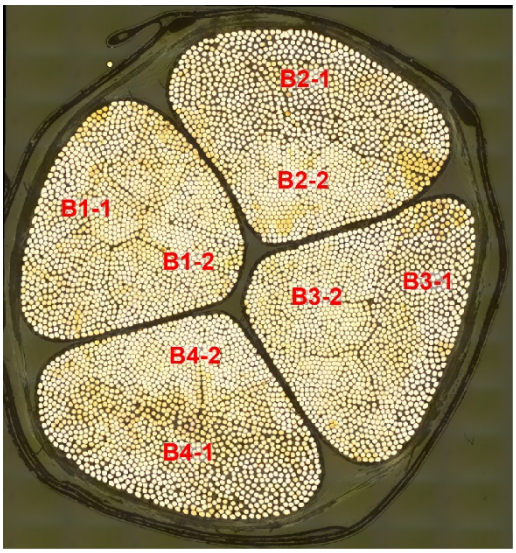

Fig. 8 Quantitative image analysis results of microstructures of as-received Litz wires [10].

model for various packings representing the system above. Fig. 9 compares conductivity and heat flux distributions in a hexagonal versus a random packing arrangement with 60% filament volume, 15% coating, and, 25% open space. This distribution is observed more towards the outer corner of each bundle where the conductor filaments were loosely packed (see Fig. 8 sections B1-1, B2-1, B3-1, and B4-1). As the individual filaments become more densely packed (i.e., 75% filament volume, 15% coating, and 10% open space; see Fig. 8 sections B1-2, B2-2, B3-2, and B4-2), the interaction between high-conductivity wires is expected to result in high heat flux concentrations in the low-conductivity potting area located between the closely spaced wires. This difference might not be significant when comparing the heat flux graphs in Figs. 9 and 10 with only about 15% difference in the filament volume fraction. However, a more notable impact on the effective transverse thermal conductivity is observed. There is an approximate 43% drop in transverse conductivity, when the filament fraction is increased from 60% to 75% in a hexagonal packing arrangement, whereas for a random packing arrangement, there is only a 22% drop in transverse conductivity. The observed higher drop in transverse conductivity for the more idealized hexagonal packing might be due to the higher number of filaments packed within a given volume in a more structured manner. For both configurations, the heat flux variation seems to be maximum at filament borders and transition sections. Axial conductivity values are also similar for various packings and are more dependent on filament percentage (as expected). Meanwhile, a closer look at hexagonal and random packings with the higher filament volume percentage (75%) shows how the heat distribution changes when the filaments are also defined as the source of heating (Fig. 5). For both packings, hot spots seem to lie in the diagonal direction, which is parallel to the equivalent stress state (here: thermal stress) in the vector mechanics law used with this platform. Filaments have never been studied as a heat source in current Literature, and more effort should be made to define them as such. The authors are taking a deeper look into this phenomenon.

A more optimized approach would be to use a randomly clustered pack (see example Fig. 11) with approximate corner and center characteristics observed in Fig. 8. The clustering function is not perfected yet in HFGMC, but it can provide us with some preliminary estimates of conductivities (see Fig. 11). More work is in progress with the clustered functionality of HFGMC. After the results are verified, the ultimate goal of the microthermal model is to help us get a better understanding of how microlevel variations can influence the macroscale results and how significant the effect would be.

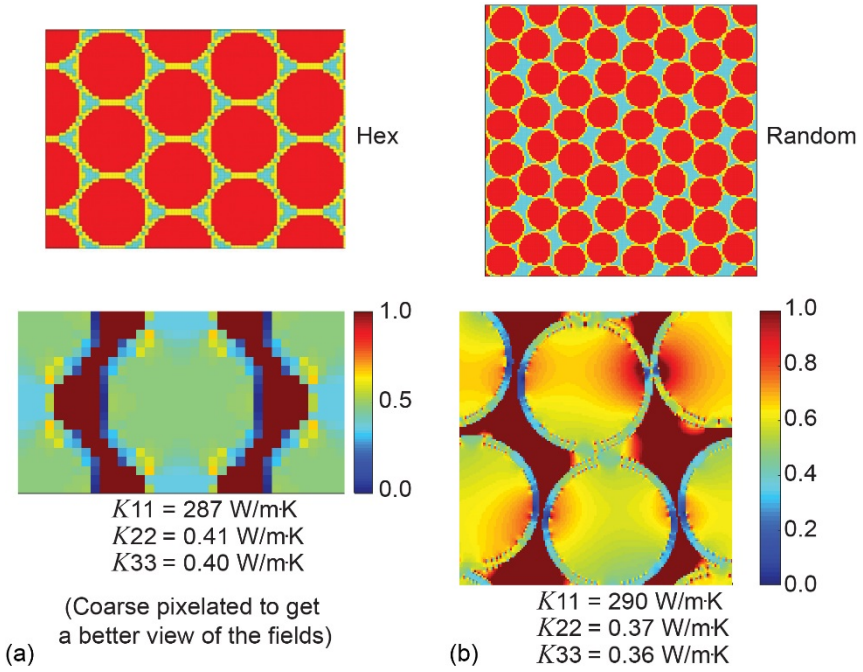

Fig. 9 Potted Litz wires of 60% filament volume, 15% coating, and 25% open space (outer corners; e.g., B1-1 from Fig. 8); computational time is ~3 s. Red is the conductor, yellow is the wire insulation, and blue is the potting material. (a) shows hexagonal packing, the ideal packing arrangement. (b) shows a randomized packing arrangement that represents a more extreme departure from the ideal case. Bottom images show the normalized heat flux map for the respective packing.

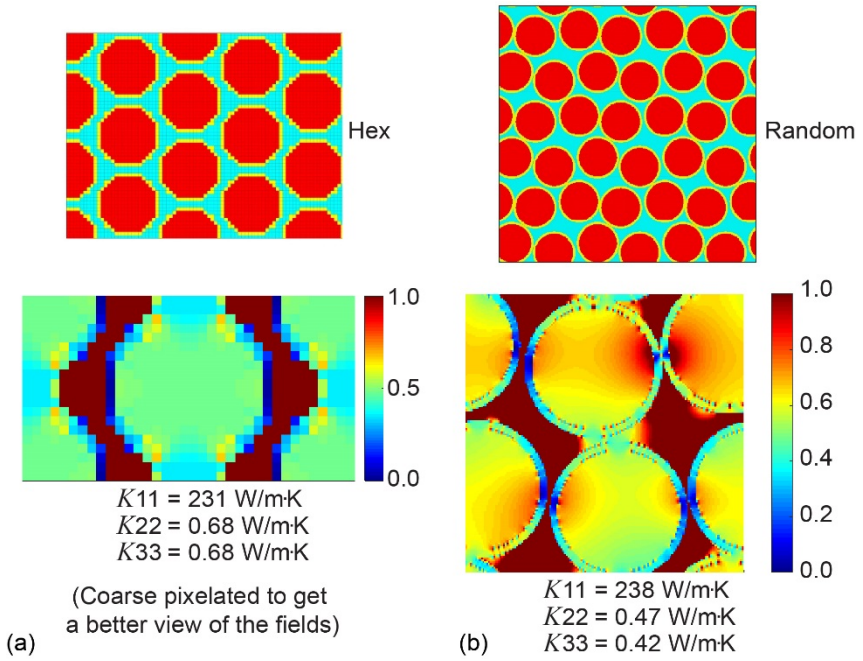

Fig. 10 Potted Litz wires of 75% filament volume, 15% coating and 10% open space (inner corners; e.g., B1-2 from Fig. 8) computational time is ~ 4 s. Red is the conductor, yellow is the wire insulation, and blue is the potting material. (a) shows hexagonal packing, the ideal packing arrangement. (b) shows a randomized packing arrangement that represents a more extreme departure from the ideal case. Bottom images show the normalized heat flux map for the respective packing.

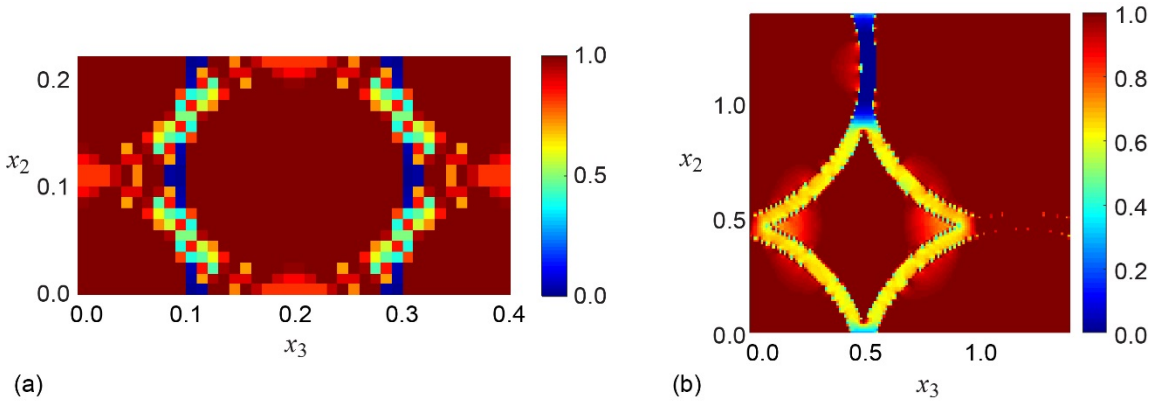

Fig. 11 A closer look at the heat flux distributions for (a) hexagonal and (b) random packings when the filaments are defined as the heat source.

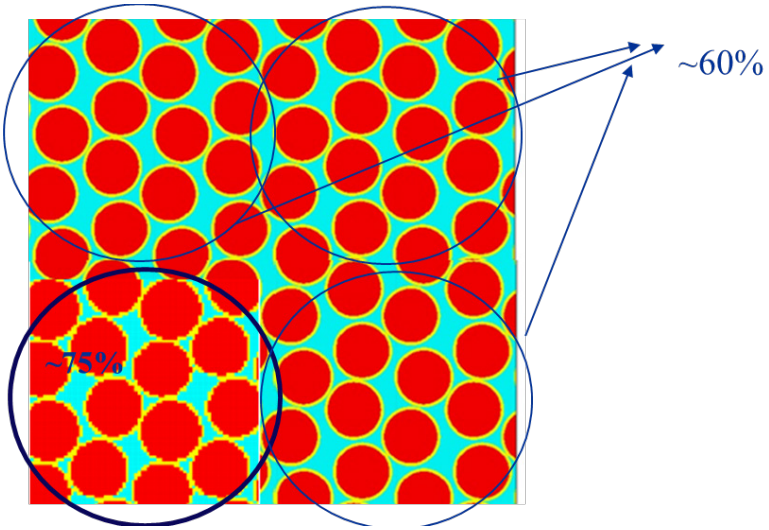

Fig. 12 Random clustered pack with approximate corner and center characteristics reported in Fig. 2.

VII. Conclusions

A significant effort was put forth to accurately replicate the thermal conditions (materials, geometry, cooling power dissipated) to those of an HEMM stator that is currently being designed for aeronautics applications. This resulted in a statorette that contains six windings of fully insulated and potted (1.3 W/m·K epoxy) type 8 Litz wire in metal laminated slots that were cooled with silicone oil kept at 60 °C to replicate the cooling environment commonly found on current aircraft. The result show that the design is able to provide adequate thermal management while passing 500 A (1048 W) without exceeding 200 °C. A transverse thermal conductivity of the Litz wire system was calculated to be 3.4 W/m·K. A conjugate thermal model was constructed and accurately predicted statorette temperatures. The results showed the value of tight packing of the Litz wire bundle and high thermal conductivity of the epoxy used for potting. Cross sectional analysis of potted Litz wire in a metal laminated slot showed thorough impregnation of the system. Microthermal analysis was applied to better capture the heat flow through the Litz wire, potting material, and insulation matrix.

Acknowledgments

This work is cosponsored by the NASA Advanced Air Transportation Technologies project and the Hybrid Gas Electric Subproject and Convergent Aeronautics Solution's HEATheR Activity and Transformative Tools and Technology project, performed at NASA Glenn Research Center. Special thanks to Daniel Scheiman and Yaritza De Jesus-Arce.

References

1. Jansen, R. H., Bowman, C., and Jankovsky, A. "Sizing power components of an electrically driven tail cone thruster and a range extender," *16th AIAA Aviation Technology, Integration, and Operations Conference, AIAA*. Vol. 3766, 2016, p. 2016.
2. Jansen, R., De Jesus-Arce, Y., Kascak, P., Dyson, R. W., Woodworth, A., Scheidler, J. J., Edwards, R., Stalcup, E. J., Wilhite, J., and Duffy, K. P. "High Efficiency Megawatt Motor Conceptual Design," *2018 Joint Propulsion Conference*. 2018, p. 4699.
3. Woodworth, A., Jansen, R., Duffy, K. P., Naghipour, P., and Shin, E. E. "Creating a multifunctional composite stator slot material system to enable high power density electric machines for electrified aircraft applications," *2018 AIAA/IEEE Electric Aircraft Technologies Symposium*. 2018, p. 5012.
4. Wereszczak, A. A., Cousineau, J. E., Bennion, K., Wang, H., Wiles, R. H., Burress, T. B., and Wu, T. "Anisotropic Thermal Response of Packed Copper Wire," *Journal of Thermal Science and Engineering Applications* Vol. 9, No. 4, 2017, p. 041006.
5. Jansen, R., Dyson, R. W., Woodworth, A., Scheidler, J. J., Smith, A. D., Stalcup, E. J., Tallerico, T., De Jesus-Arce, Y., and Avanesian, D. "High Efficiency Megawatt Motor Preliminary Design," *2018 AIAA/IEEE Electric Aircraft Technologies Symposium (EATS)*. IEEE, Indianapolis, Indiana, 2019.
6. "ANSYS Workbench with CFX and CFD-Post, Engineering Simulation Software." 19.2 ed., ANSYS Inc, Canonsburg, PA, 2019.
7. "ANSYS Workbench Mechanical, Engineering Simulation Software." 19.2 ed., ANSYS Inc, Canonsburg, PA, 2019.
8. Clearco Products Co., I. "STO-50 Silicone Transformer Oil Product Information Sheet."
9. Simpson, N., Wrobel, R., and Mellor, P. H. "Estimation of equivalent thermal parameters of impregnated electrical windings," *IEEE Transactions on Industry Applications* Vol. 49, No. 6, 2013, pp. 2505-2515.
10. Shin, E.-S. E. "Pot-ability Assessment of Litz Wires for High Power Density Electric Motor," *2018 AIAA/IEEE Electric Aircraft Technologies Symposium (EATS)*. IEEE, Indianapolis, Indiana, 2019.
11. Bednarcyk, B. A., Aboudi, J., and Arnold, S. M. "Micromechanics of composite materials governed by vector constitutive laws," *International Journal of Solids and Structures* Vol. 110, 2017, pp. 137-151. doi: 10.1016/j.ijsolstr.2017.01.033
12. Murthy, P. L., Bednarcyk, B. A., and Mital, S. K. "A Compilation of MATLAB Scripts and Functions for MACGMC Analyses," 2017.